Journal of Biomedical Optics

SPIEDigitalLibrary.org/jbo

Pressure-induced near infrared spectra response as a valuable source of information for soft tissue classification

Blaž Cugmas
Miran Bürmen
Maksimilijan Bregar
Franjo Pernuš
Boštjan Likar

SPIE

Pressure-induced near infrared spectra response as a valuable source of information for soft tissue classification

Blaž Cugmas, Miran Bürmen, Maksimilijan Bregar, Franjo Pernuš, and Boštjan Likar
University of Ljubljana, Faculty of Electrical Engineering, Laboratory of Imaging Technologies, Tržaška 25, Ljubljana SI-1000, Slovenia

Abstract. Acquiring near infrared spectra *in vivo* usually requires a fiber-optic probe to be pressed against the tissue. The applied pressure can significantly affect the optical properties of the underlying tissue, and thereby the acquired spectra. The existing studies consider these effects to be distortions. In contrast, we hypothesize that the pressure-induced spectral response is site- and tissue-specific, providing additional information for the tissue classification. For the purpose of this study, a custom system was designed for dynamic pressure control and rapid acquisition of spectra. The pressure-induced spectral response was studied at three proximate skin sites of the human hand. The diffuse reflectance and scattering were found to decrease with the applied contact pressure. In contrast, the concentrations of chromophores, and consequently the absorption, increased with the applied contact pressure. The pressure-induced changes in the tissue optical properties were found to be site-specific and were modeled as a polynomial function of the applied contact pressure. A quadratic discriminant analysis classification of the tissue spectra acquired at the three proximate skin sites, based on the proposed pressure-induced spectral response model, resulted in a high (90%) average classification sensitivity and specificity, clearly supporting the working hypothesis.
 [DOI: 10.1117/1.JBO.18.4.047002]

Keywords: spectroscopy; near infrared; pressure effects; tissue diagnostic; reflectance.

Paper 12746PR received Nov. 19, 2012; revised manuscript received Mar. 5, 2013; accepted for publication Mar. 6, 2013; published online Apr. 3, 2013.

1 Introduction

Near infrared spectroscopy (NIRS) is a rapid, noninvasive spectroscopic technique that has considerable medical diagnostic potential.[1] The numerous biomedical applications of NIRS include performing optical biopsies, detecting breast[2] and skin[3] cancer, making cancer treatment decisions, and defining therapeutic drug levels.[1] Most of these applications utilize the unique ability of NIRS to quantify the tissue chromophores, in particular hemoglobin, lipids, and water, which can be used to differentiate between normal and diseased tissue.[1] However, acquiring NIR spectra *in vivo* usually requires a fiber-optic probe to be pressed against the tissue. In general, even light pressure can significantly affect the optical properties of the underlying tissue, and thereby the acquired NIR spectra.

One of the first studies on the optical properties of the soft tissue under pressure focused on the reflectance, reduced scattering, and absorption coefficient in the spectral range from 400 to 1800 nm.[4] The soft tissue samples, including human skin, bovine aorta, and bovine and porcine sclera, were exposed to constant contact pressures of 9.8, 98, and 196 kPa. The measured reflectance changes in the NIR region were not always consistent; however, under 1400 nm, reflectance decreased with the applied pressure. In contrast, the reduced scattering and absorption coefficient were reported to increase with the applied pressure. The increase in absorption was explained by the local tissue compression, which increased the chromophore concentration; leakage of some extracellular tissue fluids; and the volumetric water content. Likewise, the increase in scattering was explained by the pressure-induced increase in the scatterer concentration.

The study of Chen et al.[5] confirmed that diffuse reflectance of the palm skin in the spectral range from 1100 to 1700 nm decreases with the applied pressure. The spectra were acquired continuously for 60 s after applying a contact pressure from 32 to 75 kPa. The diffuse reflectance spectra exhibited significant changes during the first 30 s of measurements and became stable afterward. Reflectance changes were attributed to the distortion of the internal tissue structure and chromophore distribution. Human skin of the inner forearm was investigated by Atencio et al.[6] The spectra were acquired in the spectral range from 530 to 680 nm by applying contact pressure from 0 to 10 kPa. The results were inconsistent under 600 nm, while above 600 nm, the diffuse reflectance decreased with the applied pressure. However, the results were not in agreement with the research of Randeberg,[7] where the diffuse reflectance increased with the applied pressure.

Another study reported that the changes in the soft tissue optical properties under the applied pressure are site-specific.[8] Human skin was investigated by reflectance spectroscopy in the visible spectral range. The reflectance of the neck skin decreased with the applied pressure, indicating decrease in the scattering. In contrast, the applied pressure increased the scattering of the forehead skin. The different scattering changes were explained by the fact that skull lies close to the skin surface, preventing the dermis from collapsing into the hypodermis, which results in more light reaching the dermis layers, rich in highly scattering

Address all correspondence to: Blaž Cugmas, University of Ljubljana, Faculty of Electrical Engineering, Laboratory of Imaging Technologies, Tržaška 25, Ljubljana SI-1000, Slovenia. Tel: +386 1 4768 873; Fax: +386 1 4768 279; E-mail: blaz.cugmas@fe.uni-lj.si

collagen. The absorption coefficient decreased with increasing pressure for all measurement sites. The decrease was attributed to the blood being pushed out by the applied pressure, lower perfusion, and modified tissue morphology. It was concluded that short-term (<2 s), low-contact pressure (<9 kPa) effects do not significantly affect the acquired spectra.

The existing studies used simple measurement setups during the acquisition of spectra, which exposed the sample to a constant pressure for an extended period of time. Moreover, the effects of contact pressure on the soft tissue spectra were primarily considered to be a distortion that needs to be analyzed and removed to obtain repeatable and accurate measurements. In contrast, the objective of this study was to analyze the contact pressure-induced spectral response and use the information for tissue classification. Namely, pressure-induced spectral response is tissue- and site-specific, presenting an additional useful dimension in the acquired data (Fig. 1). For the purpose of this study, a custom real-time system for rapid *in vivo* acquisition of NIR diffuse reflectance spectra of tissue under controlled contact pressure was developed. Such a measurement system enabled the study of the contact pressure-induced dynamic effects in the soft tissue. As a result, a novel model of the pressure-induced soft tissue spectral response was developed and successfully employed for the classification of three proximate skin sites on the human hand.

2 Materials and Methods

2.1 *Samples*

Measurements were conducted on the skin surface of four human volunteers (Caucasian males). Three measurement sites were chosen: namely, the palm skin above the abductor pollicis brevis muscle, skin in the middle of the wrist crease above the veins, and skin at the lateral part of the wrist above the ulnar styloid process. While the soft muscle tissue and the tissue above veins provided relatively smooth and gradually increasing resistance to the applied pressure, the tissue above the bone exhibited only limited compression. In addition, the soft tissues at the three selected sites are differently perfused and were expected to provide relevant insight into the unique tissue properties observed in the contact pressure-induced spectral response.

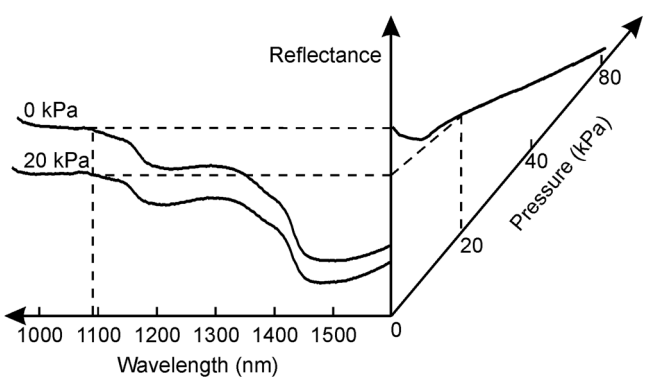

Fig. 1 Contact pressure as an additional data dimension.

2.2 *Instrumentation*

The measurement system used in this study is shown in Fig. 2. Spectra were acquired by a commercial NIR spectrometer (NIR-512L-1.7T1, 901 to 1685 nm, Control Development Inc., South Bend, Indiana) employing a broadband halogen light source (AvaLight-Hal LS, Avantes, Apeldoornseweg, the Netherlands) and a stainless steel, fiber-optic diffuse reflectance probe (Avantes, FCR-7IR400-2-ME) consisting of one detection and six illumination fibers. The diameter of the probe was 6.35 mm, so the contact pressure area was 31.7 mm^2. The probe was fixed to a metal tube, which smoothly slid through the metal rings. A force sensor (Honeywell S&C, FS01, Honeywell, Inc., Morristown, New Jersey) was attached between the end of the metal tube and the linear position sensor (9615R5.1KL2.0, 52.3 MM, Bei Sensors, Goleta, California). The travel length of the shaft spring return mechanism was 4 cm. A motorized linear stage provided precise and accurate control of the applied contact pressure.

2.3 *Measurements*

The hands of the four volunteers were fixed during the measurement process, which started by activating the motorized linear stage with a predefined motion speed. The motion was stopped when the linear position sensor exhibited full contraction, resulting in around 100 kPa of contact pressure. The spectral and pressure data were acquired synchronously at a rate of 35 Hz. Nine measurements were made at each of the three selected sites (muscle: the palm skin above the abductor pollicis brevis muscle; veins: skin in the middle of the wrist crease above the veins; bone: skin at the lateral part of the wrist above the ulnar styloid process), allowing about 5 min for the tissue to recover from the previous measurement. The 108 measurement sets obtained for the four volunteers were divided into two equal independent set (namely, the training and the test set), each containing the data collected on two volunteers.

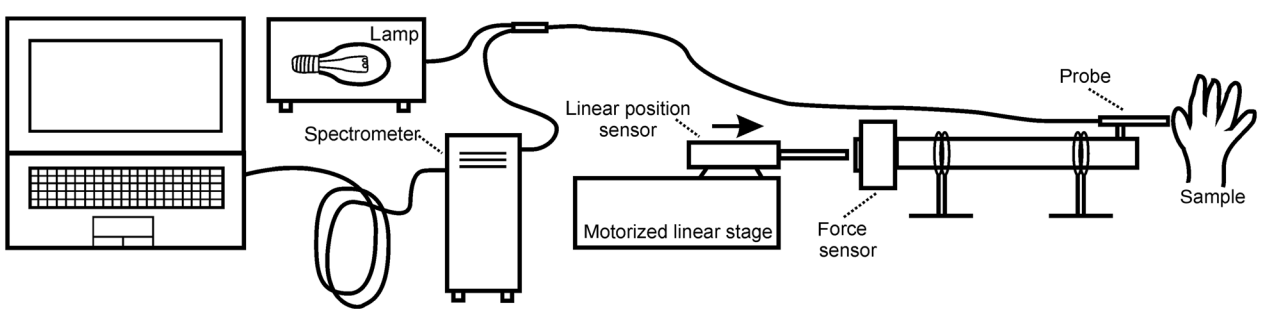

Fig. 2 Illustration of the employed measurement system.

2.4 *Spectra Processing*

All the acquired spectra were calibrated using a standard diffuse reflectance tile (Spectralon, Labsphere, North Sutton, New Hampshire). The reflectance spectra R were calculated according to the following equation:

$$R = \frac{I - D}{I_0 - D}, \tag{1}$$

where I is the acquired spectrum, D is the dark response of the sensor array, and I_0 is the spectrum of the standard diffuse reflectance tile. Due to the poor sensitivity of the employed sensor array at the lower and the upper end of the spectral range, only the spectral range from 950 to 1600 nm was used. Two different modeling approaches were employed in order to study the contact pressure-induced spectral response (Fig. 3).

The scattering and absorption properties of the tissue were estimated from the steady-state diffuse reflectance measurements in a spectrally constrained manner.[9,10] Briefly, a forward model of the diffuse reflectance R utilizing prior knowledge on the scattering and absorption properties of chromophores was used:

$$R(\lambda) = \frac{1}{4\pi}\left[z_0\left(\mu_{\text{eff}} + \frac{1}{\rho_1}\right)\frac{e^{-\mu_{\text{eff}}\rho_1}}{\rho_1^2} + (z_0 + 2z_b)\left(\mu_{\text{eff}} + \frac{1}{\rho_2}\right)\frac{e^{-\mu_{\text{eff}}\rho_2}}{\rho_2^2}\right], \tag{2}$$

where z_0, μ_{eff}, ρ_1, ρ_2, and z_b are the wavelength-dependent internal variables calculated from the absorption $\mu_a(\lambda)$ and reduced scattering $\mu_s'(\lambda)$ coefficients. The absorption coefficient was modeled as a linear combination of the chromophore concentrations:

$$\mu_a(\lambda) = c_{\text{water}}\mu_a^{\text{water}}(\lambda) + c_{\text{Hb}}[\alpha\mu_a^{\text{oxyHb}}(\lambda) + (1-\alpha)\mu_a^{\text{deoxyHb}}(\lambda)] + c_{\text{lip}}\mu_a^{\text{lip}}, \tag{3}$$

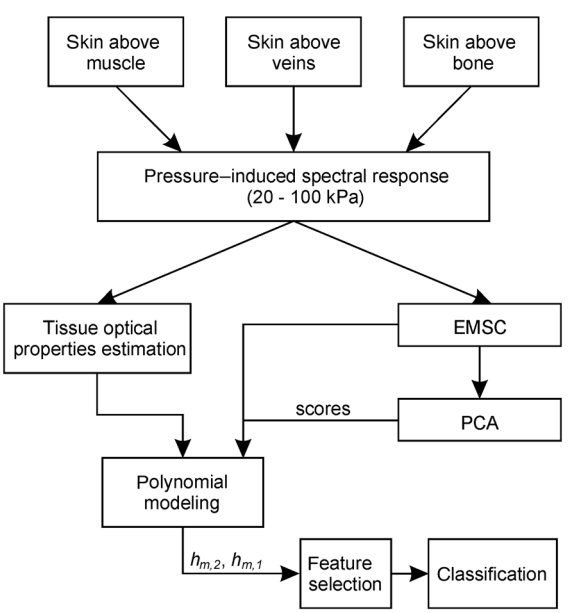

Fig. 3 Outline of the employed pressure-induced soft tissue spectral response modeling and classification.

where μ_a^{water}, μ_a^{oxyHb}, μ_a^{deoxyHb}, and μ_a^{lip} are the wavelength-dependent absorption coefficients of water, oxyhemoglobin, deoxyhemoglobin, and lipids, respectively,[11–14] c_{water}, c_{Hb}, and c_{lip} are the concentrations of water, hemoglobin, and lipids, respectively, and α is the oxygenation fraction (i.e., saturation). The reduced scattering coefficient was modeled according to the wavelength-dependent power law:

$$\mu_s' = u\lambda^{-v}, \tag{4}$$

where u is the scattering magnitude and v is the scattering power.[9,10,15]

To gain insight on the most prominent NIR absorption bands governing the pressure-induced spectral response, an additional analysis of the acquired spectra was performed. The acquired spectra were preprocessed by the extended form of multiplicative scatter correction (EMSC)[16] to roughly separate the tissue scattering and absorption properties. In contrast to the basic form of the multiplicative scatter correction (MSC),[17] EMSC considers light scattering effects as wavelength-dependent and models each acquired spectrum (r_i) according to

$$r_i = a_i + b_i r_{\text{ref}} + k_i\lambda + l_i\lambda^2, \tag{5}$$

where a_i is the baseline, b_i is the path length, r_{ref} is the reference spectrum, and k_i and l_i model the wavelength-dependent spectral variations. The EMSC coefficients (a, b, k, l) estimated by a least-squares solution were used to calculate the preprocessed spectrum r_{EMSC} as

$$r_{\text{EMSC}} = (r_i - a_i - k_i\lambda - l_i\lambda^2)/b_i. \tag{6}$$

In order to extract the spectral response induced by the applied contact pressure, the preprocessed reflectance spectra were subjected to the principal component analysis (PCA) followed by a detailed analysis of the spectral bands highlighted by the calculated PCA loading.

The estimated concentrations of chromophores (c_{water}, c_{Hb}, and c_{lip}), the scattering magnitude u and the scattering power v, the oxygenation fraction α, the estimated EMSC coefficients (a, b, k, l), and the calculated PCA scores s of the EMSC preprocessed spectra were modeled by a polynomial function of the applied contact pressure p:

$$m = \sum_{j=0}^{N} h_{m,j}p^j + e, \qquad m \in \{c_{\text{water}}, c_{\text{Hb}}, c_{\text{lip}}, u, v, \alpha, a, b, k, l, s_1, s_2, \ldots, s_{N_s}\}, \tag{7}$$

where e is the fit error. The calculated polynomial coefficients h_m (without the $h_{m,0}$) were used to form the feature vectors, employed by the subsequent quadratic discriminant analysis (QDA)[18]—based classification into three classes corresponding to the three selected measurement sites. The optimal feature subsets for the two modeling approaches were selected by the sequential forward-floating selection algorithm (SFFS),[19] minimizing the average classification error rate of the training set. The classification sensitivity and specificity were estimated by the independent test set. It should be stressed that only the relative spectral changes were used in this study. Therefore, the polynomial coefficients $h_{m,0}$, which were not affected by the applied contact pressure, were not used for the classification.

In order to compare the contact pressure-induced spectral response with the findings of other studies, the mean reflectance, the reduced scattering, and absorption coefficients (1450 nm) were modeled by a first-order polynomial function of the applied contact pressure [Eq. (7)].

3 Results and Discussion

3.1 *General Findings*

The chromophore concentrations, oxygenation fraction, and the scattering magnitude and power were estimated by fitting each acquired reflectance spectrum to the model [Eq. (2)] in a least-squares sense [Fig. 4(a)], while the PCA scores s were calculated after applying EMSC preprocessing. The spectra exhibited significant and frequently inconsistent changes [Fig. 4(b)] for the contact pressure under 16 kPa. In general, the mean reflectance dropped significantly after the probe touched the skin. However, some of the acquired spectra did not exhibit any obvious change. The diversity of observed spectral changes may be attributed to two main mechanisms. First, the initial light coupling improves with the increasing pressure, gradually leading to a firm contact between the probe and the skin. Second, the contact pressure under the normal blood pressure of 120 mm Hg (16 kPa) substantially affects the blood flow in the upper tissue layers. At higher contact pressure, the light coupling does not improve anymore. However, the pressure is gradually transferred to the deeper tissue layers. Because of that, more and more blood is pushed out of the tissue. Consequently, the spectra exhibit substantial linear and higher-order dependence on the applied contact pressure.

For the above-explained reasons, only the contact pressure range from 20 to 100 kPa, where the spectral changes were found consistent [Fig. 4(b)], was used by the subsequent analysis. The chromophore concentrations, oxygenation fraction, and the reduced scattering magnitude u and power v were modeled by a first-order polynomial, while the PCA scores exhibited slight nonlinearity, requiring a second-order polynomial model.

3.2 *Classification*

Five of the six features describing the tissue scattering and absorption properties (Fig. 3) were selected by the SFFS method for the classification. Only the polynomial coefficient corresponding to the hemoglobin concentration was not. This was somewhat expected, as the hemoglobin absorption in the NIR spectral range is relatively low compared to the absorption of water and lipids. Moreover, the applied contact pressure in excess of 16 kPa removes most of the blood from the underlying tissue. In contrast, only three features, the two polynomial coefficients estimating the first PCA score and the quadratic polynomial coefficient estimating the EMSC parameter k, were selected for the classification based on the second modeling approach. The classification results are summarized in Table 1. The average classification sensitivity and specificity and posterior probability for the first model were 81% and 73%, respectively. The second model exhibited similar classification posterior probability (74%) and slightly better average sensitivity and specificity (90%). The classification specificity was the highest for the skin above the bone (100%), while the highest classification sensitivity was observed for the wrist (100%).

3.3 *Tissue Scattering and Absorption Properties as a Linear Function of the Applied Contact Pressure*

For all 108 acquired measurement sets, the diffuse reflectance and reduced scattering coefficient at 1450 nm decreased with the applied contact pressure. In contrast, the absorption coefficient at 1450 nm consistently increased with the applied contact pressure. The average reflectance and absorbance changes were in accordance with the majority of the existing studies.[4–6] However, Lim et al.[8] reported that the reduced scattering coefficient of the forehead skin increased with the applied pressure. The explanation was that the skull prevents the dermis from collapsing into the hypodermis, and therefore light can penetrate deeper into the tissue rich with the highly scattering collagen. Skin on the forehead can be considered similar to the skin above the ulnar styloid process, which was used in this study. However, no increase in the scattering was observed.

The slopes of the linear polynomial model corresponding to the selected features are listed in Table 2. The variability of the calculated slopes was the smallest for the skin above the muscle tissue and the highest for the skin above the veins. At

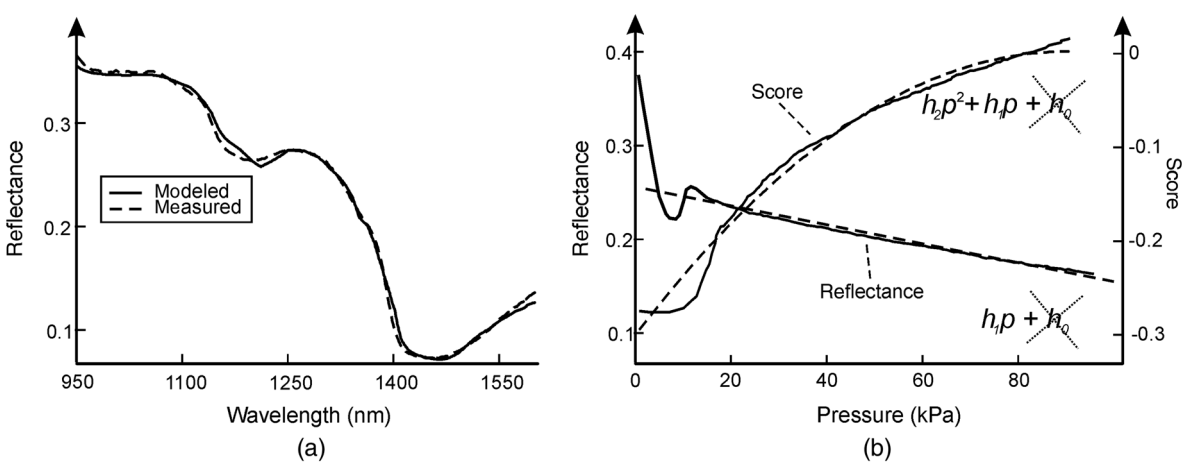

Fig. 4 (a) Example of a measured and modeled [Eq. (2.)] reflectance spectrum. (b) Example of a mean reflectance and PCA score as a function of the applied contact pressure (solid line) and the corresponding polynomial fit (dashed line) calculated for the contact pressure from 20 to 100 kPa.

Table 1 Classification sensitivity and specificity and the corresponding posterior probability obtained by polynomial modeling of the tissue absorption and scattering properties (A) and PCA scores (B).

	Average		Skin above muscle		Skin above veins		Skin above bone	
	Sensitivity and specificity	Posterior probability	Sensitivity	Specificity	Sensitivity	Specificity	Sensitivity	Specificity
A	0.81	0.73	0.61	0.92	0.89	0.81	0.72	0.89
B	0.90	0.74	0.78	0.94	1.00	0.86	0.83	1.00

Table 2 Median value and the corresponding range between the 25th and 75th percentile (brackets) of the polynomial slope.

Feature	Skin above muscle	Skin above veins	Skin above bone
Mean reflectance (10^{-4} kPa^{-1})	−1.20 [−1.44 −0.94]	−2.49 [−2.69 −2.09]	−1.80 [−2.18 −1.20]
Abs. coef. ($\mu_a^{1450\ nm}$) (10^{-3} mm^{-1} kPa^{-1})	1.45 [0.90 1.77]	1.17 [0.41 2.34]	1.22 [0.94 1.96]
Red. scat. coef. ($\mu_s'^{1450\ nm}$) (10^{-2} mm^{-1} kPa^{-1})	−0.51 [−0.77 −0.33]	−1.56 [−5.80 −0.73]	−0.94 [−1.67 −0.67]
Water conc. (c_{water}) (10^{-3} kPa^{-1})	3.51 [2.11 4.41]	2.98 [1.03 5.87]	3.05 [2.38 4.84]
Saturation (α) (10^{-3} kPa^{-1})	−0.59 [−0.85 −0.39]	−2.78 [−5.07 −1.66]	−2.18 [−3.05 −1.20]
Lipid conc. (c_{lip}) (10^{-3} kPa^{-1})	7.00 [3.78 11.03]	5.45 [1.16 12.09]	8.38 [4.95 11.94]
Sc. magnitude (u) (10^{-3} kPa^{-1})	1.31 [0.72 2.42]	3.13 [2.29 3.99]	3.85 [2.62 5.63]
Sc. power (v) (10^{-4} kPa^{-1})	3.09 [1.92 3.93]	5.46 [2.72 8.59]	4.74 [3.58 6.84]
Score 1 (s_1) (10^{-5} kPa^{-1})	−3.67 [−5.52 −1.07]	−7.23 [−8.62 −5.35]	1.54 [0.42 2.57]
EMSC coef. (k) (kPa^{-1})	1.87 [0.39 2.74]	1.99 [1.25 2.80]	0.45 [−0.05 0.87]

the wrist, the tendons and bones are close to veins, so the tissue structure can vary significantly; hence, the measurement repeatability is lower. On the other hand, the muscle tissue structure is more homogeneous, resulting in higher measurement repeatability.

The highest reflectance decrease was observed above the veins, while the reflectance decrease observed above the muscle tissue was more than two times smaller (Fig. 5). The skin above the muscle tissue also exhibited the highest increase in absorption at 1450 nm, indicating the dominant impact of scattering on the reflectance. The absorption increase observed above the muscle tissue was attributed to the increase in the concentration of water and lipids. During the measurements, the muscle provided less resistance to the applied pressure; therefore, the skin under the probe sagged deeper. As a result, the relative change in the concentration of water (Fig. 5) and lipids was higher compared to the tissue above the veins and bone, where the contact pressure was distributed to a smaller tissue volume. The differences in the tissue structure are also responsible for the higher oxygen saturation drop (Fig. 5) observed above the veins and bone. The reduced scattering coefficient consistently decreased with the contact pressure, most prominently above the veins (Fig. 5). The scattering decrease could be explained by the decrease in the refractive index mismatch due to the water displacement in the dermis and epidermis.[8]

3.4 *Analysis of the PCA Loadings*

A detailed analysis of the PCA loadings confirmed the findings based on the results obtained by modeling the tissue scattering and absorption properties and gave additional insight on the most prominent NIR absorption bands governing the pressure-induced spectral response. The first PCA loading of the EMSC preprocessed skin pressure-induced spectral response (shown in Fig. 6) exhibits three distinct absorption bands. Two absorption bands, centered at 1210 and 1170 nm, can be attributed to the absorption of lipid mixture,[13] which was shown to have a significant absorption band centered at 1210 nm, and a minor absorption band centered at 1170 nm, both in excellent agreement with the absorption bands highlighted by the first PCA loading. With respect to the wavelength dependence of the reduced scattering coefficient and the EMSC preprocessing of the acquired spectra, it is reasonable to assume that the calculated loadings predominantly reflect the pressure-induced changes in the absorption properties of the underlying tissue, and thereby concentration of the chromophores. Under the assumption that the lipids cannot be pushed out of the tissue by the applied pressure, the concentration of lipids can change only as a result of the increase or decrease in the relative volume fractions of the chromophores. This supposition is clearly supported by the third, water-related[11] absorption band of the first

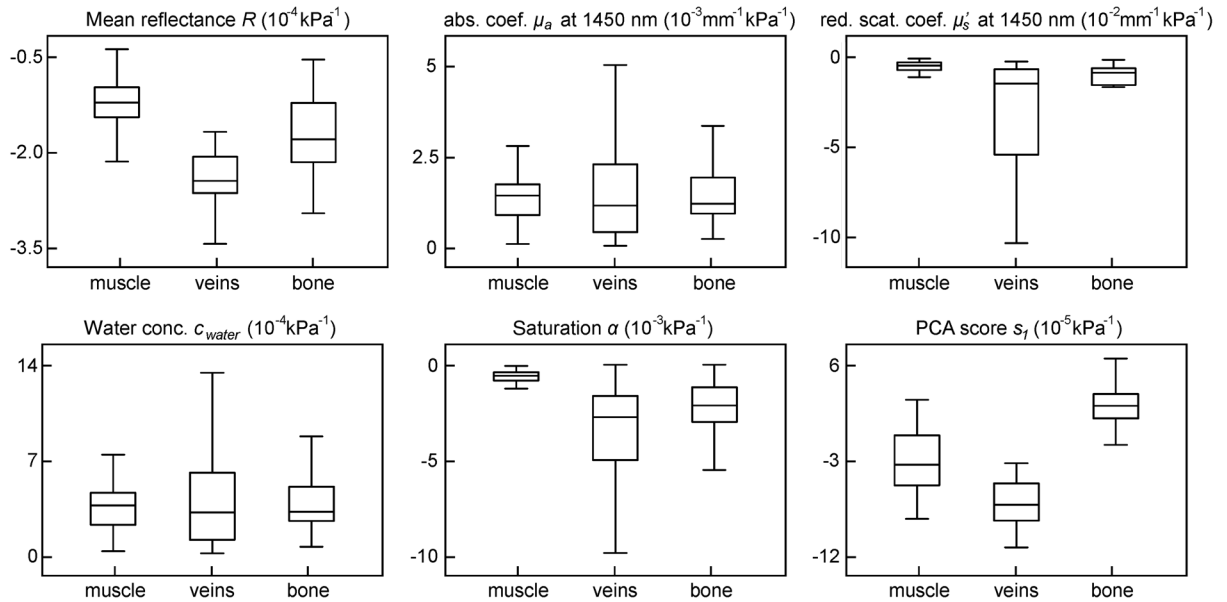

Fig. 5 Slopes (h_1) of the selected features (Table 2) modeled as a polynomial function of the applied contact pressure for the three measurement sites: skin above the muscle (muscle), skin in the middle of the wrist crease above the veins (veins) and skin above the ulnar process (bone).

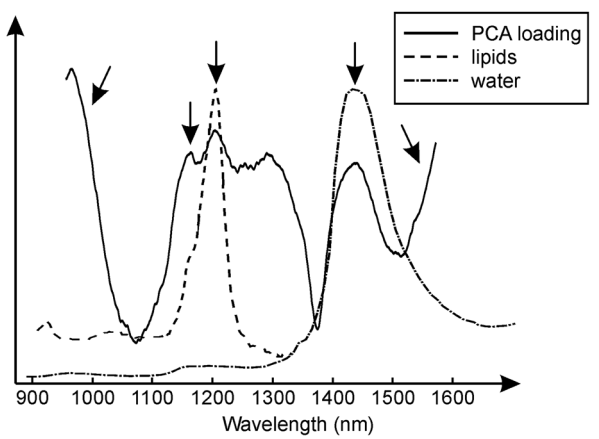

Fig. 6 First PCA loading of the skin spectra (full line). Absorption spectrum of water (dash-dotted line) and absorption spectrum of lipids (dashed line from 900 to 1350 nm). The absorption bands of lipids (1170 nm and 1210 nm) and water (1450 nm) are depicted by the vertical arrows. The absorption bands of hemoglobin are depicted by the inclined arrows.

PCA loading observed at 1450 nm. Additionally, a decrease in the value of the first PCA loading at the locations (depicted by the two inclined arrows in Fig. 6) was observed. According to Kuenstner and Norris,[12] different hemoglobin species have absorption bands located in the spectral range from 800 to 1100 nm and in the spectral range from 1500 to 1600 nm (oxyhemoglobin at 924 nm, deoxyhemoglobin at 903 nm, and methemoglobin at 1017 nm), all in excellent agreement with the two depicted locations.

4 Conclusions

This study showed for the first time that pressure-induced spectral response of the soft tissue in the NIR spectral range can be used as a valuable source of additional information for tissue classification. Even though the measurements were acquired at three proximate skin locations, the subcutaneous tissue provided unique spectral response to the applied pressure. In general, the applied contact pressure increased the concentrations of chromophores (water, hemoglobin, and lipids), resulting in higher absorbance and lower diffuse reflectance and scattering. The proposed classification scheme, utilizing solely a pressure-induced spectral response by polynomial modeling of the tissue scattering and absorption properties, resulted in a high (90%) average classification sensitivity and specificity. Based on the presented results, the NIR, pressure-induced spectral response of the soft tissue indicates considerable potential for improving the sensitivity and specificity of soft tissue classification.

Acknowledgments

This work was supported by the Ministry of Higher Education, Science and Technology, Republic of Slovenia under Grants L2-4072, J7-2246, and L2-2023.

References

1. V. R. Kondepati, H. M. Heise, and J. Backhaus, "Recent applications of near-infrared spectroscopy in cancer diagnosis and therapy," *Anal. Bioanal. Chem.* **390**(1), 125–139 (2008).
2. B. J. Tromberg et al., "Imaging in breast cancer—Diffuse optics in breast cancer: detecting tumors in pre-menopausal women and monitoring neoadjuvant chemotherapy," *Breast Cancer Res.* **7**(6), 279–285 (2005).
3. L. M. McIntosh et al., "Towards non-invasive screening of skin lesions by near infrared spectroscopy," *J. Invest. Dermatol.* **116**(1), 175–181 (2001).
4. E. K. Chan et al., "Effects of compression on soft tissue optical properties," *IEEE J. Sel. Top. Quant.* **2**(4), 943–950 (1996).
5. W. L. Chen et al., "Influence of contact state on NIR diffuse reflectance spectroscopy in vivo," *J. Phys. D-Appl. Phys.* **38**(15), 2691–2695 (2005).
6. J. A. D. Atencio et al., "Influence of probe pressure on human skin diffuse reflectance spectroscopy measurements," *Opt. Mem. Neural Networks* **18**(1), 6–14 (2009).
7. L. L. Randeberg, "Diagnostic applications of diffuse reflectance spectroscopy," Doctoral Thesis, Norwegian University of Science and

Technology, Faculty of Information Technology, Mathematics and Electrical Engineering (2005).
8. L. Lim et al., "Probe pressure effects on human skin diffuse reflectance and fluorescence spectroscopy measurements," *J. Biomed. Opt.* **16**(1), 011012 (2011).
9. J. Sun et al., "Influence of fiber optic probe geometry on the applicability of inverse models of tissue reflectance spectroscopy: computational models and experimental measurements," *Appl. Opt.* **45**(31), 8152–8162 (2006).
10. A. Kim and B. C. Wilson, "Measurement of ex vivo and in vivo tissue optical properties: methods and theories," in *Optical-Thermal Response of Laser-Irradiated Tissue*, Springer, Netherlands (2011).
11. D. J. Segelstein, "The complex refractive index of water," Master's Thesis, University of Missouri (1981).
12. J. Kuenstner and K. Norris, "Spectrophotometry of human hemoglobin in the near infrared region from 1000 to 2500 nm," *J. Near. Infrared Spec.* **2**(1), 59–65 (1994).
13. C. L. Tsai, J. C. Chen, and W. J. Wang, "Near-infrared absorption property of biological soft tissue constituents," *J. Med. Biol. Eng.* **21**(1), 7–14 (2001).
14. G. B. Altshuler, R. R. Anderson, and D. Manstein, "Method and apparatus for the selective targeting of lipid-rich tissue," U. S. Patent No. 6,605,080 B1 .
15. A. N. Bashkatov et al., "Optical properties of human skin, subcutaneous and mucous tissues in the wavelength range from 400 to 2000 nm," *J. Phys. D-Appl. Phys.* **38**(15), 2543 (2005).
16. H. Martens, J. P. Nielsen, and S. B. Engelsen, "Light scattering and light absorbance separated by extended multiplicative signal correction. Application to near-infrared transmission analysis of powder mixtures," *Anal. Chem.* **75**(3), 394–404 (2003).
17. P. Geladi, D. MacDougall, and H. Martens, "Linearization and scatter-correction for near-infrared reflectance spectra of meat," *Appl. Spectrosc.* **39**(3), 491–500 (1985).
18. T. Næs et al., *User Friendly Guide to Multivariate Calibration and Classification*, NIR Publications, Chichester (2002).
19. P. Pudil, J. Novovičová, and J. Kittler, "Floating search methods in feature selection," *Pattern Recogn. Lett.* **15**(11), 1119–1125 (1994).